Efficient Assembly of Bridged β-Ga_2O_3 Nanowires for Solar-Blind Photodetection

By *Yanbo Li, Takero Tokizono, Meiyong Liao, Miao Zhong, Yasuo Koide, Ichiro Yamada,* and *Jean-Jacques Delaunay**

An increasing number of applications using ultraviolet radiation have renewed interest in ultraviolet photodetector research. Particularly, solar-blind photodetectors sensitive to only deep UV (<280 nm), have attracted growing attention because of their wide applicability. Among recent advances in UV detection, nanowire (NW)-based photodetectors seem promising, however, none of the reported devices possesses the required attributes for practical solar-blind photodetection, namely, an efficient fabrication process, a high solar light rejection ratio, a low photocurrent noise, and a fast response. Herein, the assembly of β-Ga_2O_3 NWs into high-performance solar-blind photodetectors by use of an efficient bridging method is reported. The device is made in a single-step chemical vapor deposition process and has a high 250-to-280-nm rejection ratio (~2×10^3), low photocurrent fluctuation (<3%), and a fast decay time (<<20 ms). Further, variations in the synthesis parameters of the NWs induce drastic changes in the photoresponse properties, which suggest a possibility for tuning the performance of the photodetectors. The efficient fabrication method and high performance of the bridged β-Ga_2O_3 NW photodetectors make them highly suitable for solar-blind photodetection.

1. Introduction

The extremely harmful ultraviolet C (UVC, 100–280 nm) radiation cannot penetrate the earth's protective atmosphere and, therefore, UVC is not part of solar radiation at the Earth's surface. The absence of UVC in solar radiation and artificial lighting provides a "black background" for detection of weak UVC emitting sources such as flames. Accordingly, selective detection of UVC without sensitivity to solar radiation has been named solar-blind photodetection. Solar-blind photodetectors have found many civil and military applications including fire detection, missile warning, non-line-of-sight optical communication, chemical/biological analysis, and UV astronomy.[1–3] Unfortunately, the commercially available solar-blind detectors are based on the photoelectric effect (photomultiplier tubes), which requires high operating voltages, thus limiting their applications.

Current research in solar-blind photodetectors focuses on UVC sensitive wide band gap semiconductors such as $Al_xGa_{1-x}N$, $Mg_xZn_{1-x}O$, diamond, AlN, cubic BN, and the monoclinic gallium oxide (β-Ga_2O_3).[4–9] Epitaxially grown $Al_xGa_{1-x}N$ should be fabricated with $x \geq 0.45$ to achieve solar-blind photodetection, but the quality of the $Al_xGa_{1-x}N$ films deteriorates rapidly as the Al content increases.[2] The wurtzite $Mg_xZn_{1-x}O$ can only be synthesized for $x \leq 0.37$ due to phase segregation between ZnO wurtzite and MgO rock salt which results in a maximum bandgap of 4.3 eV, not large enough for solar-blind photodetection.[10] Diamond, AlN, and cubic BN on the contrary have very large band gaps of 5.5, 6.1, and 6.3 eV, which limit their detection to wavelengths shorter than 225, 210, and 193 nm, respectively.[6–8] The β-Ga_2O_3 with a band gap of ~4.5 eV is particularly suitable for solar-blind photodetection.[11–13] β-Ga_2O_3 single crystals have been used to fabricate Schottky photodiodes for solar-blind photodetection.[14,15] Recently, the use of nanostructured materials for photon detection has attracted much attention.[16–19] For instance, ZnO nanowires (NWs) have been demonstrated to have very high photoconductive gain due to their one-dimensional structure and charge separation properties.[20] On the other hand, the β-Ga_2O_3 NWs have been synthesized by various groups and their fundamental properties have been studied.[21–24] To the best of our knowledge, only one study has been conducted on the fabrication of solar-blind photodetector with β-Ga_2O_3 NWs.[25] The reported photodetector was made from a single β-Ga_2O_3 NW by top-down techniques resorting to photolithography for the fabrication of the metallic electrodes. The device exhibited high sensitivity and fast response to 254 nm light. However, the photocurrent was noisy due to the high Schottky barrier and the spectral selectivity of the device was not reported.

[*] Y. B. Li, T. Tokizono, M. Zhong, Prof. I. Yamada, Prof. J.-J. Delaunay
Department of Mechanical Engineering
School of Engineering
The University of Tokyo
7–3-1 Hongo, Bunkyo-ku, Tokyo, 113–8656 (Japan)
E-mail: jean@mech.t.u-tokyo.ac.jp
Dr. M. Y. Liao, Prof. Y. Koide
Sensor Materials Center
National Institute for Materials Sciences (NIMS)
Namiki 1–1, Tsukuba, Ibaraki, 305–0044 (Japan)

DOI: 10.1002/adfm.201001140

© 2010 WILEY-VCH Verlag GmbH & Co. KGaA, Weinheim

The conventional top-down approach for fabrication of NW-based devices is complicated, time-consuming, and expensive and, therefore, is limited to fundamental studies and laboratory demonstrations. To extend the field of applications of NW-based devices, a more efficient and practical method is needed to assemble NWs into functional devices.[26–28] In our previous work, we have developed a single-step bridging method to assemble bridged ZnO NWs into visible-blind photodetectors.[29–31] The bridged NW device has been demonstrated to have several advantages over the conventional NW devices: 1) the fabrication process is simple, efficient, and cost-effective; 2) the NW surfaces are free from contamination because no post-process is needed after the growth of the bridged NWs (e.g., resist coating for photolithography); 3) the NW properties are not affected by the substrate because the bridged NWs are not in contact with the substrate, unlike the situation in conventional NW devices; 4) the structure is free of contact barriers because the bridged NWs and their electrodes (consisting of thick NW layers) are made of the same material during the same growth process. In this report, we show that the bridging method can be applied to assemble β-Ga_2O_3 NWs into a bridged structure which exhibited high performance in solar-blind photodetection. A stable and high photocurrent with a photocurrent to dark current ratio of ~3×10^4 was achieved under 2 mW cm^{-2} at a wavelength of 254 nm. A fast photocurrent decay with a characteristic time of much less than 20 ms was observed. In addition, a clear cutoff wavelength at ~280 nm and a high 250-to-280-nm rejection ratio of ~2×10^3 were obtained. The photoluminescence (PL) properties of the β-Ga_2O_3 NWs were also investigated, showing the intrinsic UVC emissions for the first time. To further understand the photoresponse mechanism, bridged β-Ga_2O_3 NWs having different defect densities were synthesized and their photoresponse and PL properties were investigated. The results revealed that the photoresponses of the β-Ga_2O_3 NWs can be tailored to meet the needs of different applications for the photodetectors.

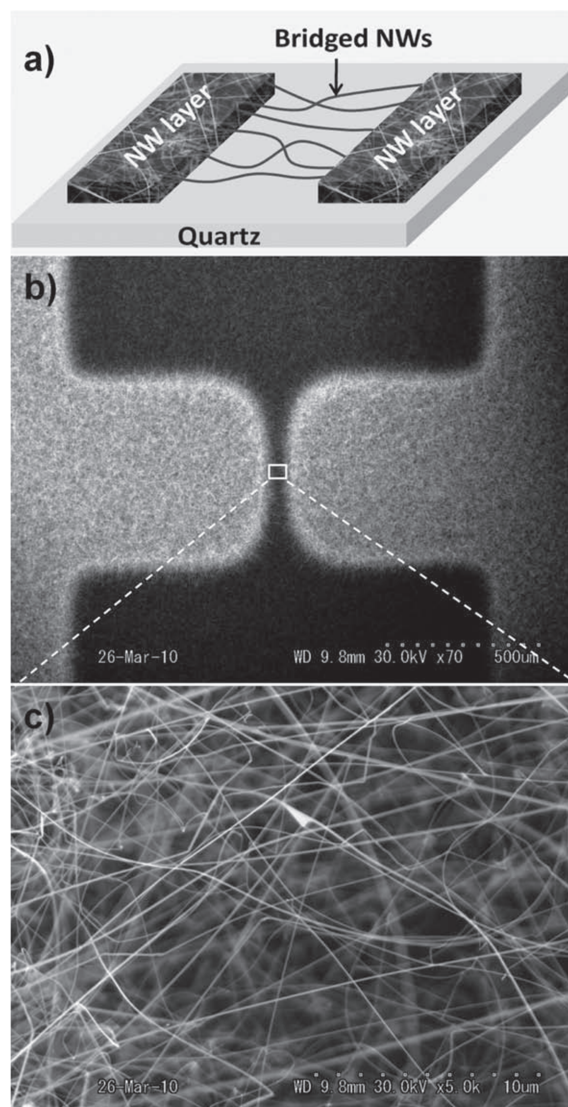

Figure 1. a) Schematic diagram of the bridged NW structure showing the electrodes made of thick β-Ga_2O_3 NW layers and the bridged NWs crossing the gap between the NW electrodes. b) An SEM image of the bridged β-Ga_2O_3 NW structure. c) A magnified view of the bridged β-Ga_2O_3 NWs crossing the gap.

2. Results and Discussion

2.1. Fundamental Properties of β-Ga_2O_3 NWs

Figure 1a shows a schematic diagram of the bridged NW structure. The structure consists of thick NW layers, serving as native electrodes, and, bridged NWs across the gap between the thick layers, acting as sensing elements. The NW layer electrodes and the bridged NWs are synthesized simultaneously in a single-step chemical vapor deposition (CVD) process. In order to achieve selective growth of β-Ga_2O_3 NW layers, very thin (~2 nm) Au layers having the shape of the electrodes are patterned by sputtering Au through a physical mask on quartz substrates. Bridged NWs are formed across the gap between the NW layer electrodes in a self-grown process. Figure 1b shows a scanning electron microscope (SEM) image of the bridged β-Ga_2O_3 NW structure synthesized at a substrate temperature of 1000 °C. The SEM image clearly shows the selective growth of β-Ga_2O_3 NW layers on the patterned Au layers. The shape of the thick NW layers is defined by the shape of the thin Au layers. A magnified view of the gap area between the NW layers in Figure 1c shows that the electrodes are bridged by many NWs. The bridged β-Ga_2O_3 NWs have diameters of several tens of nanometers and lengths up to one hundred micrometers. The β-Ga_2O_3 NWs most likely grew by a vapor-solid process, because no Au particles were found at the tips of the NWs.

The X-ray diffraction (XRD) pattern of **Figure 2** reveals that the NWs are indeed crystalline β-Ga_2O_3. All the diffraction peaks can be indexed with those of the monoclinic β-Ga_2O_3 with lattice parameters a = 1.223 nm, b = 0.304 nm, c = 0.580 nm, and β = 103.7° (JCPDS Card No. 43–1012). **Figure 3a** shows the high-resolution transmission electron microscope (TEM) image of a β-Ga_2O_3 NW with a diameter of ~60 nm grown at 1000 °C. The magnified image of the core part of the NW in Figure 3b reveals lattice fringes with a d-spacing of 0.58 nm, which

© 2010 WILEY-VCH Verlag GmbH & Co. KGaA, Weinheim

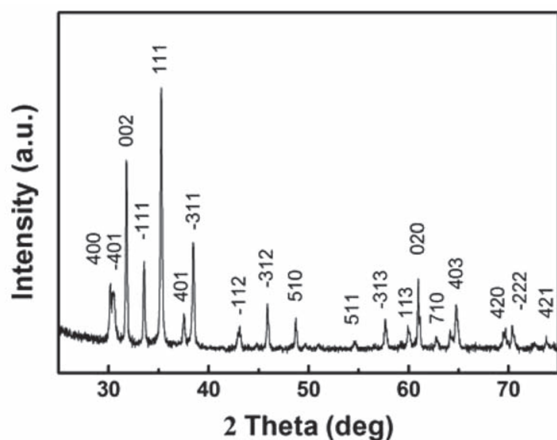

Figure 2. XRD pattern of the β-Ga_2O_3 NWs. All the diffraction peaks can be indexed to the monoclinic phase β-Ga_2O_3 (JCPDS Card No. 43–1012).

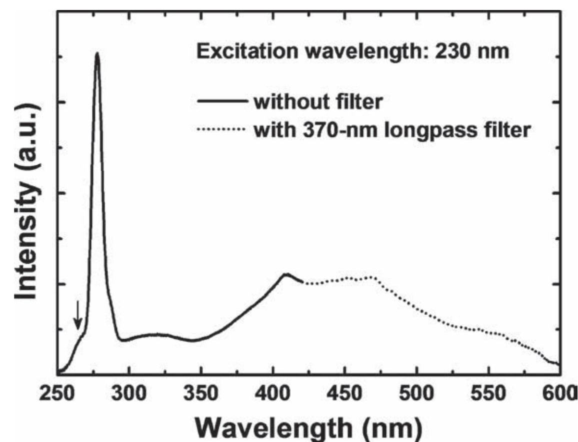

Figure 4. Room-temperature PL spectrum of the β-Ga_2O_3 NWs grown at 1000 °C (Sample 1). The arrow indicates the shoulder in the shorter wavelength side of the UVC emission.

matches that of the (001) lattice planes of β-Ga_2O_3. The NW is found to grow along the [001] direction, in consistence with the selected-area electron diffraction (SAED) pattern recorded along the [100] axis shown in Figure 3d. The TEM image of Figure 3c is evidence for the presence of an amorphous surface layer with a thickness of ~3 nm. This amorphous layer contrasts with the highly ordered lattice in the core of the NW and may play an important role in the photoresponse process.

The room-temperature PL spectrum of the β-Ga_2O_3 NWs synthesized at 1000 °C (denoted as Sample 1) is shown in **Figure 4**. The PL spectrum shows a strong UVC emission and multiple emissions in the UVA to the visible range. Detailed view of the UVC emission reveals a weak peak at ~265 nm (~4.7 eV) besides the main peak at ~278 nm (~4.5 eV). Both peaks should be intrinsic emissions of β-Ga_2O_3 that originate from the anisotropy of the monoclinic phase. Indeed, Ueda *et al*. showed by optical transmission spectroscopy that β-Ga_2O_3 had two absorption edges at 4.79 and 4.52 eV for light polarized with E//b and E//c, respectively.[13] The band gaps obtained from our PL spectrum are in good agreement with the band gaps estimated from their optical transmission spectra. Previous studies of the PL properties of β-Ga_2O_3 single crystals[32,33] and nanostructures[21–23,34–35] show only blue emission or UVA emission, with no intrinsic emission in the UVC range. To the best of our knowledge, this is the first time the intrinsic PL emission is observed for β-Ga_2O_3. The observation of the intrinsic emission may be explained by improved crystal quality of our NWs and/or the use of proper excitation source (λ = 230 nm). The PL spectrum of our sample also shows several defect emissions in the UVA to visible range (350–600 nm) with intensities lower than that of the intrinsic emission. These defect emissions may arise from the donor levels to acceptor levels electron-hole recombination. It has been proposed that the donor levels are induced by the oxygen vacancies and the acceptor levels are formed by gallium vacancies or gallium-oxygen vacancy pairs.[21,36] According to Binet and Gourier,[32] electrons in donor clusters forming donor levels are captured via a tunnel transfer process by holes on acceptor levels to form trapped excitons, which recombine radiatively emitting photons. The tunnel transfer process is slower than the radiative recombination process and, therefore, determines the recombination rate for the defects emissions. This has significant influence on the photoresponse properties of β-Ga_2O_3 NWs with different defect densities.

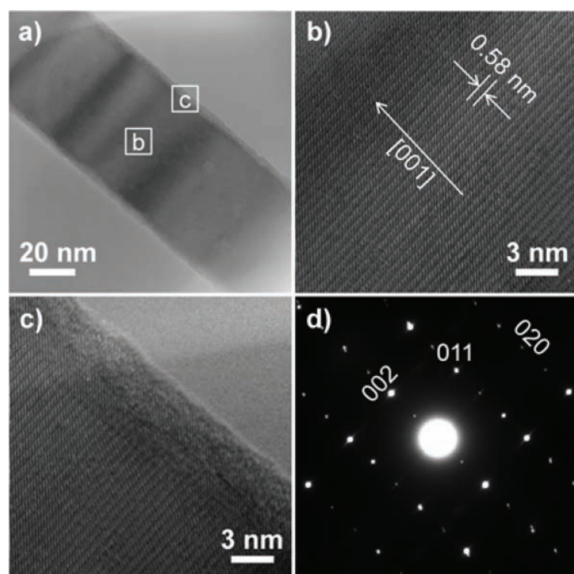

Figure 3. a) High-resolution TEM image of a β-Ga_2O_3 NW grown along the [001] axis. Magnified images of b) the box b and c) the box c as indicated in figure a), revealing a good crystallinity of the NW core and a thin amorphous surface layer, respectively. d) SAED pattern of the NW recorded along the [100] axis.

2.2. Photoresponse Properties of the Bridged β-Ga_2O_3NWs

The photoresponse properties of the bridged β-Ga_2O_3 NWs were studied in controlled conditions to eliminate the disturbances caused by changes in the environment conditions such as temperature and humidity. The temperature was kept at ~20 °C and the relative humidity was kept below 15%. **Figure 5a** shows a representative time-dependent photoresponse of the bridged

© 2010 WILEY-VCH Verlag GmbH & Co. KGaA, Weinheim

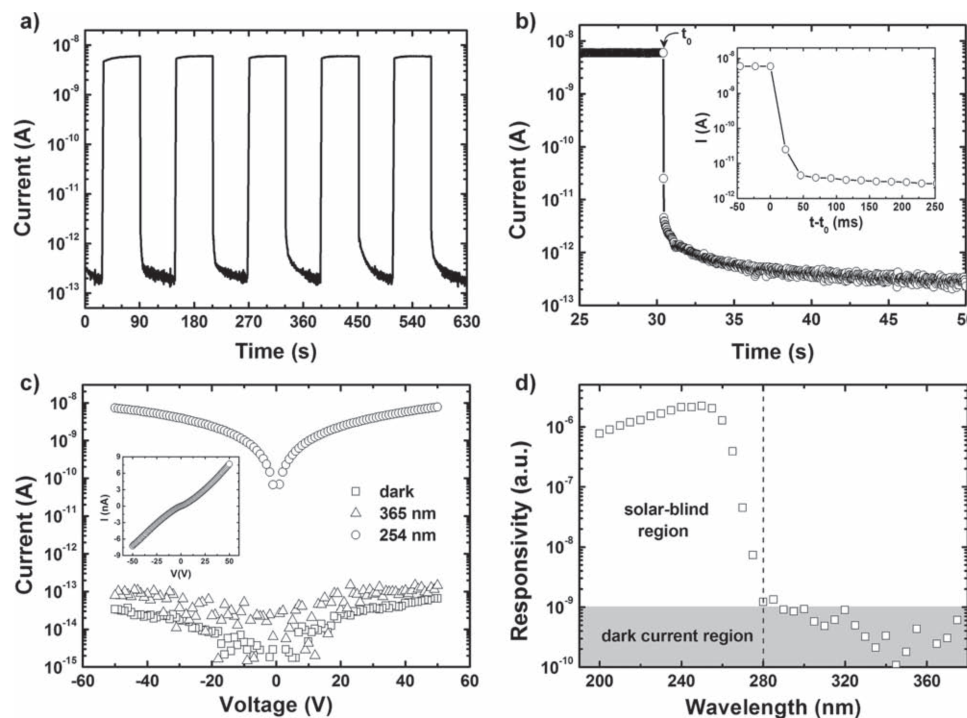

Figure 5. Photoresponse properties of the bridged β-Ga_2O_3 NWs grown at 1000 °C (Sample 1). a) Time-dependent photoresponse of the bridged β-Ga_2O_3 NWs measured in dry air under UVC (~2 mW cm^{-2} at 254 nm) illumination with a period of 60 s at a bias voltage of 50 V.[36] The photocurrent to dark current ratio was ~3×10^4. b) Photocurrent decay process of the device. The inset shows the enlarged decay edge. c) *I–V* characteristics of the bridged β-Ga_2O_3 NWs in dark (squares), under 365 nm light (triangles), and under 254 nm light (circles). The *I–V* curve measured under 254 nm light is plotted on a linear scale in the inset. d) Spectral response of the bridged β-Ga_2O_3 NWs revealing that the device is blind to solar light. The dashed line indicates the lowest wavelength of the solar spectrum on Earth.

β-Ga_2O_3 NWs (Sample 1). Under a bias voltage of 50 V,[37] the dark current was only ~0.2 pA. This extremely low dark current is favorable for practical sensing devices. Upon UVC (254 nm) illumination, the current instantaneously increased by more than 4 orders of magnitude to ~6 nA. A photocurrent to dark current ratio of ~3×10^4 is achieved under an irradiance of ~2 mW cm^{-2}. Soci *et al.* have demonstrated that the surface states causing charge separation were responsible for the high photoconductive gain in ZnO NWs.[20] The high photoconductivity of the β-Ga_2O_3 NWs may be attributed to the surface states arose from the amorphous surface layer observed in the TEM image of Figure 3c. The surface states serve as trapping centers for the photogenerated holes, cause charge separation, and prolong the lifetime of the photogenerated electrons. Besides the high photoconductivity, the photocurrent of our device is less noisy in comparison with the photocurrent of the single β-Ga_2O_3 NW photodetector of Ref. 25 under similar measurement bandwidths (~10 Hz). The photocurrent fluctuation ($\Delta I/\bar{I}$, as defined in Ref. 26) of our device is less than 3% at a bias voltage of 5 V (see Supporting Information Figure S2). This result contrasts with the over 30% photocurrent fluctuation for the single β-Ga_2O_3 NW photodetector fabricated by photolithography.[25] Generally, the photocurrent noise in barrier-type photodetectors is attributed to the flicker noise (intrinsic noise), the random electron-hole generation/recombination, and the noise generated by the fluctuation of the potential barrier that controls the electron injection from the electrodes into the conduction band of the photoconducting material (photoinduced noise).[38] In our device, the extremely low dark current of the bridged β-Ga_2O_3 NW photodetector indicates that the intrinsic noise is very small. In the single β-Ga_2O_3 NW photodetector, the Schottky barrier between the NW and the Au electrodes should be very high, judging from the reported highly nonlinear current–voltage (*I–V*) curve under UVC illumination. Consequently, the photoinduced noise is very high and is the main contribution to the photocurrent noise. On the contrary, in our device the NW-layer electrodes and the bridged NWs are free of barrier because they are made of the same material, and the barriers between the indium contacts and the NW-layer electrodes are very low. Therefore, the photoinduced noise is very small in our device. The small intrinsic noise and small photoinduced noise resulted in a stable photocurrent in our bridged β-Ga_2O_3 NW photodetector.

Figure 5b shows a typical photocurrent decay process of the bridged β-Ga_2O_3 NW photodetector. The current decreased by more than two orders of magnitude within ~20 ms (integration time of each points) and decreased to the dark level within ~10 s. The persistent photoconductivity (PPC) effect, which is usually seen in photoconducting materials such as ZnO and GaN,[30,39] was not observed in the bridged β-Ga_2O_3 NWs. The PPC effect, characterized by a very slow decay process, is mainly attributed to the surface states that act as trapping centers. In ZnO and GaN, high density of surface states are formed by adsorbed oxygen ions because a large amount of electrons are available

© 2010 WILEY-VCH Verlag GmbH & Co. KGaA, Weinheim

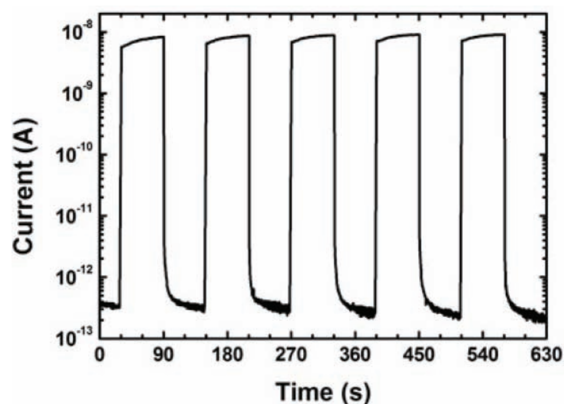

Figure 6. Time-dependent photoresponse of the bridged β-Ga_2O_3 NWs (Sample 1) measured in an argon atmosphere under the same bias voltage (50 V) and illumination conditions (~2 mW cm^{-2} at 254 nm) as in Figure 5a.

for oxygen molecules to capture. Therefore, oxygen adsorption greatly affects their photoresponse. On the contrary, the electron density of β-Ga_2O_3 NWs is extremely low. Consequently, only a low density of surface states can be created by adsorbed oxygen ions and thus oxygen adsorption has a minor effect on the photoresponse of β-Ga_2O_3 NWs. To verify this point, we have conducted photoresponse measurements in argon (Ar) atmosphere. The photoresponse curve measured in Ar shown in **Figure 6** is almost identical to that of Figure 5a measured in dry air. Especially, the decay process in Ar is found to be as fast as in air. This is in sharp contrast to the decay process of ZnO photodetectors measured in an oxygen-deficient environment, which is much slower than in air.[40–41] The bridged β-Ga_2O_3 NWs are expected to exhibit the same photoresponse properties in a vacuum as in dry air. The dark current was found to increase with increasing humidity because of the formation of a conducting water layer on the surface of the NWs. Therefore, for practical applications the device can be vacuum-packaged, protecting itself from the influence of humidity, and thus ensuring long-term and stable operation.

I–V characteristics of the bridged β-Ga_2O_3 NWs in dark and under different illumination conditions are shown in Figure 5c. Under 254 nm light, the *I–V* curve is symmetric and nearly linear as seen in the inset of Figure 5c. This confirms that the potential barrier in the bridged NW structure is very low. The *I–V* curve measured under 365 nm light does not show significant increase as compared with the *I–V* curve measured in dark, which suggests the bridged β-Ga_2O_3 NWs are not sensitive to 365 nm light. To further characterize the spectral selectivity of the bridged β-Ga_2O_3 NWs, the spectral response of the device was measured. Under light with a wavelength longer than 280 nm, the current is kept on the dark current level and the device shows nearly no response. The current begins to increase abruptly at ~275 nm, a wavelength corresponding to the band gap of the β-Ga_2O_3 NWs as estimated from the PL spectrum. High responsivity is obtained for wavelengths from 200 to 260 nm. Interestingly, the maximum responsivity is found to be at ~250 nm, which corresponds to the absorption edge of β-Ga_2O_3 obtained by polarized transmission spectroscopy with the polarization being *E*//*b*.[33] A large 250-to-280 nm rejection ratio of ~2×10^3 is obtained, which is much higher than that of the Schottky photodiode realized with a single-crystal β-Ga_2O_3 (250-to-280 nm rejection ratio of ~20).[14] The above results demonstrate that the bridged β-Ga_2O_3 NWs can be used as solar-blind photodetectors with high sensitivity and fast on/off response.

2.3. Varying the Photoresponse Properties of the Bridged β-Ga_2O_3 NWs

To further understand the photoresponse mechanism of the β-Ga_2O_3 NWs, bridged β-Ga_2O_3 NWs were fabricated under different substrate temperatures. Sample 2 and 3 were synthesized at 925 and 800 °C, respectively. These two samples synthesized at lower temperatures are expected to have more defects than Sample 1 synthesized at the higher temperature of 1000 °C. The increase in defects densities should change the photoresponse properties of the bridged β-Ga_2O_3 NWs. Indeed, the time-dependent photoresponse curves in **Figure 7a** show large changes as compared with that of Sample 1 of Figure 5a. With decreasing growth temperature, it is found that the dark conductivity and the photoconductivity increase, the photocurrent to dark current ratio increases, and the decay time increases. All these changes can be well explained by taking into account the role of defects in the β-Ga_2O_3 NWs. The PL spectra shown in Figure 7c reveal that the defect emissions are greatly enhanced with decreasing growth temperature. The PL results show that the β-Ga_2O_3 NWs have higher defect densities under lower growth temperatures. As discussed before, the defects emissions result from a two-step recombination process: 1) the tunnel transfer of electrons from donor clusters to acceptors to form trapped excitons and 2) the radiative recombination of these excitons at the acceptor sites. The tunnel transfer step is the rate determining step and was found to be much slower than the recombination process.[32] A rather long decay with a characteristic time from hundreds of microseconds to a few milliseconds was found for the defects emissions.[32,36] On the contrary, the intrinsic emission does not rely on the tunnel transfer process and therefore decays very fast with a characteristic time of less than 1 ms.[32,42] The difference in the decay times of the defect emissions and the intrinsic emission suggests that the lifetimes of the carriers in conduction and valence bands are much shorter than the lifetimes of the carriers on the defects (donor and acceptor) levels. Therefore, the changes in the photoresponse properties observed for the samples with different defect densities can be explained. The increase in the dark conductivity with increasing defects density is due to the increase in the carrier density in the β-Ga_2O_3 NWs. The increase in the photoconductivity with increasing defects density is attributed to the long lifetimes of the carriers trapped on the defects levels. This also accounts for the longer decay process in samples with higher defects densities. The spectral response of Sample 2 and Sample 3 were also measured and are reproduced in Figure 7b. For Sample 2 with intermediate defect densities, the bridged β-Ga_2O_3 NWs are insensitive to light with wavelength longer than 320 nm. The responsivity curve increases gradually in the range of 320–280 nm and increases abruptly from 275 nm. The

© 2010 WILEY-VCH Verlag GmbH & Co. KGaA, Weinheim

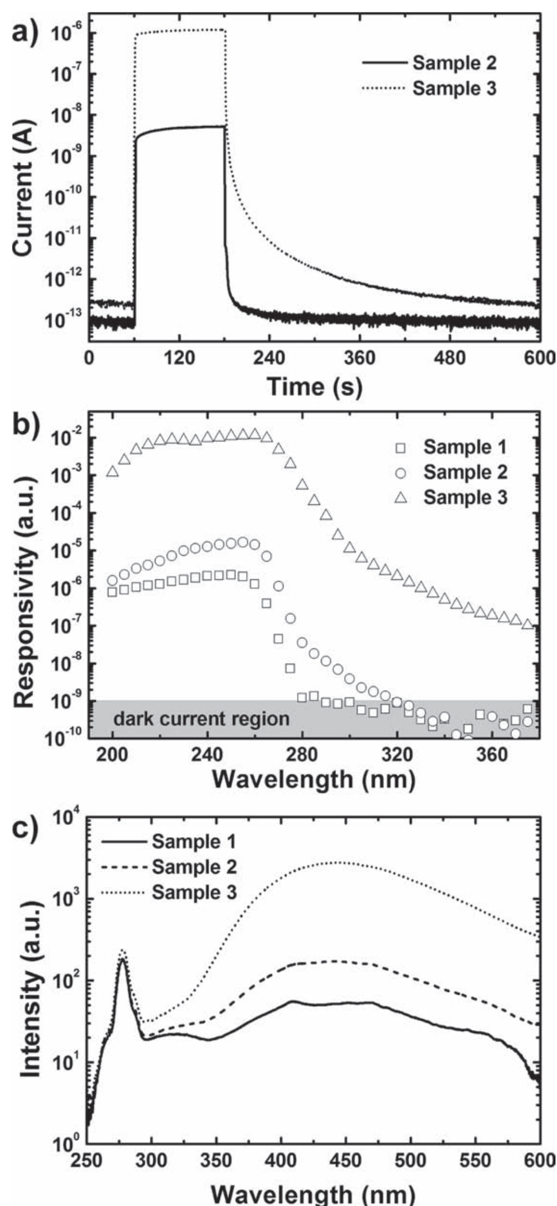

Figure 7. a) Time-dependent photoresponse of the bridged β-Ga_2O_3 NWs grown at 925 °C (Sample 2, solid line) and at 800 °C (Sample 3, dotted line) measured in dry air under a bias voltage of 5 V and an UVC (254 nm) irradiance of ~2 mW cm^{-2}. The photocurrent to dark current ratios for Sample 2 and Sample 3 were ~5×10^4 and ~5×10^6, respectively. b) Spectral responses of Sample 1 (squares), Sample 2 (circles), and Sample 3 (triangles). c) Room-temperature PL spectra of Sample 1 (solid line), Sample 2 (dashed line), and Sample 3 (dotted line), revealing an increase in defect emissions with decreasing growth temperature.

maximum responsivity increases by one order of magnitude as compared with that of Sample 1. The 250-to-280 nm rejection ratio is still as high as ~5×10^2. For Sample 3 with very high defect densities, although the maximum responsivity increases by four orders of magnitude compared to that of Sample 1, the bridged β-Ga_2O_3 NWs become sensitive to visible light and no clear cutoff wavelength is observed. The 250-to-280 nm rejection ratio is only ~20. Therefore, the effect of defects densities in the β-Ga_2O_3 NWs could be used to develop photodetectors for different applications. For photodetectors with high spectral selectivity and fast response, the defects densities in the β-Ga_2O_3 NWs should be kept at a low level. For photodetectors with high responsivity, the β-Ga_2O_3 NWs should be synthesized with high defects densities.

3. Conclusions

In conclusion, we have successfully assembled β-Ga_2O_3 NWs into a bridged structure in a single-step CVD process. The PL of the β-Ga_2O_3 NWs showed intrinsic UVC emissions, which were observed for the first time. The bridged β-Ga_2O_3 NWs exhibited a stable photocurrent ($\Delta I/\bar{I} < 3\%$), a high photocurrent to dark current ratio (~3×10^4), and a fast decay ($\tau << 20$ ms) in response to 254 nm light. Moreover, the device also showed solar-blind spectral response with a high 250-to-280-nm rejection ratio of ~2×10^4. To further understand the photoresponse mechanism, bridged β-Ga_2O_3 NWs with different defects densities were synthesized at different growth temperatures. By combining their photoresponse properties with their PL properties, it was found that the defects formed by oxygen vacancies or gallium vacancies played an important role in the photoresponse. The properties of the bridged β-Ga_2O_3 NWs could be tailored to achieve high spectral selectivity and fast response with low defect densities and to achieve high responsivity with high defect densities. Our method provides an efficient way to assemble bridged β-Ga_2O_3 NWs solar-blind photodetectors, which could find wide applications in fields such as flame detection, missile tracking, and space-to-space communications.

4. Experimental Section

Fabrication of the Bridged β-Ga_2O_3 NWs: Au pads with a thickness of ~2 nm were sputtered on quartz substrates through a metal physical mask. The distance between two facing pads was ~100 µm. β-Ga_2O_3 NWs were then grown on the substrates by CVD in a horizontal vacuum tube furnace (MTI GSL-1600X). A 0.4 g powder mixture of Ga_2O_3 and graphite (1:1 in weight) was loaded in an alumina boat as the source materials and placed at the center of the furnace. The substrate was placed 15–20 cm away from the source and downstream of the carrier gases. Argon and oxygen with a volume ratio of 20:1 were used as the carrier gases at a working pressure of ~60 Torr. The temperature of the furnace was raised to the target temperature at a rate of 10 °C min^{-1}. The temperature of the source was kept at 1180 °C for 30 min, while the temperature of the substrate was 800–1000 °C, depending on its position in the tube furnace. The substrate temperatures for Sample 1, Sample 2, and Sample 3 were 1000 °C, 925 °C, and 800 °C, respectively. After the growth, the furnace was cooled down naturally to room-temperature.

Characterization of the Fundamental Properties the β-Ga_2O_3 NWs: SEM images of the fabricated nanostructures were taken with a Hitachi S-3000N. TEM images and SAED patterns were taken with a JEOL JEM-2010F under an acceleration voltage of 200 kV. The XRD pattern of the β-Ga_2O_3 NWs was obtained with a diffractometer (MXP3, MAC Science) using a monochromatic CuKα radiation. The PL spectra of the β-Ga_2O_3 NWs were measured with a fluorescence spectrometer (FP-6600, JASCO) under excitation with a Xe lamp (excitation wavelength of 230 nm). The PL spectra in the range of 250–420 nm and 400–600 nm were taken without and with a 370-nm longpass filter, respectively. The two spectra were merged to get the full spectrum in the range of 250–600 nm.

© 2010 WILEY-VCH Verlag GmbH & Co. KGaA, Weinheim

Characterization of the Photoresponse Properties of the Bridged β-Ga_2O_3 NWs: In order to shield the electrical noise and control the gas atmosphere, the samples were installed in a tailor-made metallic chamber with a quartz window and gas inlet/outlet. The NW-layer electrodes were contacted with indium metal because indium is known to form Ohmic contact with β-Ga_2O_3[14]. The chamber was purged by dry air or argon before the measurements. The *I–V* curves and the current-time curves were recorded with a picoammeter/voltage source (6487, Keithley). The time-dependent photoresponse curves were measured using a UV transilluminator (LMS-20E, 3UV) as the light source (254 nm). The spectral photoresponse curves were measured under a bias voltage of 50 V using the excitation light of a fluorescence spectrometer (FP-6600, JASCO) as the light source. The UV light irradiances were measured with an optical power meter (PD300-UV, Ophir).

Supporting Information

Supporting Information is available from the Wiley Online Library or from the author.

Acknowledgements

This work was supported through the Global COE Program, "Global Center of Excellence for Mechanical Systems Innovation," the Asahi Glass Foundation, the Nippon Sheet Glass Foundation for Materials Science and Engineering, and Grants-in-Aid for Scientific Research (B) 22360056 from the Ministry of Education, Culture, Sports, Science and Technology (MEXT), Japan. Part of this work was conducted in the Center for Nano Lithography & Analysis, The University of Tokyo, supported by the MEXT, Japan. The authors thank Prof. Kazunari Domen and Prof. Jun Kubota (Department of Chemical System Engineering, The University of Tokyo) for the PL and spectral photoresponse measurements.

Received: June 5, 2010
Revised: July 16, 2010
Published online:

[1] M. Razeghi, A. Rogalski, *J. Appl. Phys.* **1996**, *79*, 7433.
[2] M. Razeghi, *Proc. IEEE* **2002**, *90*, 1006.
[3] E. Monroy, F. Omnes, F. Calle, *Semicond. Sci. Tech.* **2003**, *18*, R33.
[4] D. Walker, V. Kumar, K. Mi, P. Sandvik, P. Kung, X. H. Zhang, M. Razeghi, *Appl. Phys. Lett.* **2000**, *76*, 403.
[5] T. Takagi, H. Tanaka, S. Fujita, *Jpn. J. Appl. Phys., Part 2* **2003**, *42*, L401.
[6] M. Y. Liao, Y. Koide, J. Alvarez, *Appl. Phys. Lett.* **2005**, *87*, 022105.
[7] R. Dahal, J. Li, Z. Y. Fan, M. L. Nakarmi, T. M. A. Tahtamouni, J. Y. Lin, H. X. Jiang, *Phys. Status Solidi C* **2008**, *5*, 2148.
[8] A. Soltani, H. A. Barkad, M. Mattalah, B. Benbakhti, J. C. De Jaeger, Y. M. Chong, Y. S. Zou, W. J. Zhang, S. T. Lee, A. BenMoussa, B. Giordanengo, J. F. Hochedez, *Appl. Phys. Lett.* **2008**, *92*, 053501.
[9] T. Oshima, T. Okuno, N. Arai, N. Suzuki, S. Ohira, S. Fujita, *Appl. Phys. Express* **2008**, *1*, 011202.
[10] I. Takeuchi, W. Yang, K. S. Chang, M. A. Aronova, T. Venkatesan, R. D. Vispute, L. A. Bendersky, *J. Appl. Phys.* **2003**, *94*, 7336.
[11] M. Passlack, E. F. Schubert, W. S. Hobson, M. Hong, N. Moriya, S. N. G. Chu, K. Konstadinidis, J. P. Mannaerts, M. L. Schnoes, G. J. Zydzik, *J. Appl. Phys.* **1995**, *77*, 686.
[12] Z. Hajnal, J. Miro, G. Kiss, F. Reti, P. Deak, R. C. Herndon, J. M. Kuperberg, *J. Appl. Phys.* **1999**, *86*, 3792.
[13] N. Ueda, H. Hosono, R. Waseda, H. Kawazoe, *Appl. Phys. Lett.* **1997**, *71*, 933.
[14] T. Oshima, T. Okuno, N. Arai, N. Suzuki, H. Hino, S. Fujita, *Jpn. J. Appl. Phys.* **2009**, *48*, 011605.
[15] R. Suzuki, S. Nakagomi, Y. Kokubun, N. Arai, S. Ohira, *Appl. Phys. Lett.* **2009**, *94*, 222102.
[16] G. Konstantatos, E. H. Sargent, *Nat. Nanotechnol.* **2010**, *5*, 391.
[17] T. Zhai, X. Fang, M. Liao, X. Xu, L. Li, B. Liu, Y. Koide, Y. Ma, J. Yao, Y. Bando, D. Golberg, *ACS Nano* **2010**, *4*, 1596.
[18] T. Y. Zhai, X. S. Fang, M. Y. Liao, X. J. Xu, H. B. Zeng, B. Yoshio, D. Golberg, *Sensors* **2009**, *9*, 6504.
[19] L. Li, P. Wu, X. Fang, T. Zhai, L. Dai, M. Liao, Y. Koide, H. Wang, Y. Bando, D. Golberg, *Adv. Mater.* **2010**, *22*, 3161.
[20] C. Soci, A. Zhang, B. Xiang, S. A. Dayeh, D. P. R. Aplin, J. Park, X. Y. Bao, Y. H. Lo, D. Wang, *Nano Lett.* **2007**, *7*, 1003.
[21] C. H. Liang, G. W. Meng, G. Z. Wang, Y. W. Wang, L. D. Zhang, S. Y. Zhang, *Appl. Phys. Lett.* **2001**, *78*, 3202.
[22] T. I. Shin, H. J. Lee, W. Y. Song, S. W. Kim, M. H. Park, C. W. Yang, D. H. Yoon, *Nanotechnology* **2007**, *18*, 345305.
[23] C. L. Kuo, M. H. Huang, *Nanotechnology* **2008**, *19*, 155604.
[24] J. Y. Li, L. S. Wang, D. B. Buchholz, R. P. H. Chang, *Nano Lett.* **2009**, *9*, 1764.
[25] P. Feng, J. Y. Zhang, Q. H. Li, T. H. Wang, *Appl. Phys. Lett.* **2006**, *88*, 153107.
[26] M. C. P. Wang, B. D. Gates, *Mater. Today* **2009**, *12*, 34.
[27] X. S. Fang, Y. Bando, M. Y. Liao, T. Y. Zhai, U. K. Gautam, L. Li, Y. Koide, D. Golberg, *Adv. Funct. Mater.* **2010**, *20*, 500.
[28] R. S. Chen, S. W. Wang, Z. H. Lan, J. T. H. Tsai, C. T. Wu, L. C. Chen, K. H. Chen, Y. S. Huang, C. C. Chen, *Small* **2008**, *4*, 925.
[29] Y. B. Li, F. Della Valle, M. Simonnet, I. Yamada, J. J. Delaunay, *Nanotechnology* **2009**, *20*, 045501.
[30] Y. B. Li, F. Della Valle, M. Simonnet, I. Yamada, J. J. Delaunay, *Appl. Phys. Lett.* **2009**, *94*, 023110.
[31] Y. B. Li, A. Paulsen, I. Yamada, Y. Koide, J. J. Delaunay, *Nanotechnology* **2010**, *21*, 295502.
[32] L. Binet, D. Gourier, *J. Phys. Chem. Solids* **1998**, *59*, 1241.
[33] K. Shimamura, E. G. Villora, T. Ujiie, K. Aoki, *Appl. Phys. Lett.* **2008**, *92*, 201914.
[34] L. Dai, X. L. Chen, X. N. Zhang, A. Z. Jin, T. Zhou, B. Q. Hu, Z. Zhang, *J. Appl. Phys.* **2002**, *92*, 1062.
[35] S. C. Vanithakumari, K. K. Nanda, *Adv. Mater.* **2009**, *21*, 3581.
[36] T. Harwig, F. Kellendonk, *J. Solid State Chem.* **1978**, *24*, 255.
[37] We used a bias voltage of 50 V in order to characterize the dark current. For practical applications, the device can be operated under a few volts. The photoresponse properties are essentially the same under different bias voltages since the *I–V* curve is nearly linear (see Supporting Information Figure S1).
[38] A. Carbone, P. Mazzetti, *Phys. Rev. B* **1994**, *49*, 7592.
[39] C. H. Qiu, J. I. Pankove, *Appl. Phys. Lett.* **1997**, *70*, 1983.
[40] Q. H. Li, T. Gao, Y. G. Wang, T. H. Wang, *Appl. Phys. Lett.* **2005**, *86*, 123117.
[41] J. P. Cheng, Y. J. Zhang, R. Y. Guo, *J. Cryst. Growth* **2008**, *310*, 57.
[42] G. Blasse, A. Bril, *J. Phys. Chem. Solids* **1970**, *31*, 707.

© 2010 WILEY-VCH Verlag GmbH & Co. KGaA, Weinheim